Electronic Supplementary Information

Branched conjugated polymers for fast capacitive storage of sodium ions

Shuaifei Xu,[a] Hongyang Li,[b] Yuan Chen,[a] Yanchao Wu,[a] Cheng Jiang,[a] Erjing Wang*[b] and Chengliang Wang*[a]

a. School of Optical and Electronic Information, Wuhan National Laboratory for Optoelectronics (WNLO), Huazhong University of Science and Technology, Wuhan, 430074, China. E-mail: clwang@hust.edu.cn

b. Hubei Collaborative Innovation Center for Advanced Organic Chemical Materials, Ministry-of-Education Key Laboratory for the Green Preparation and Application of Functional Materials, Faculty of Materials Science and Engineering, Hubei University, Wuhan, 430062, China. E-mail: wangej@hubu.edu.cn

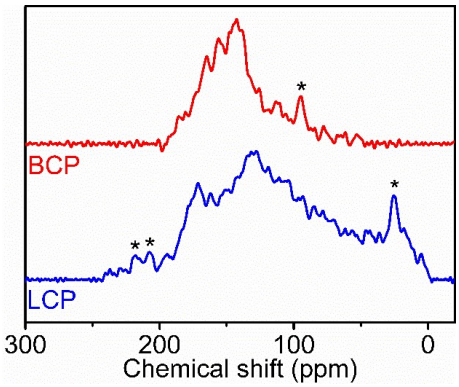

Fig. S1 Solid-state ^{13}C NMR of two polymers. The peaks marked by * are spinning side peaks.

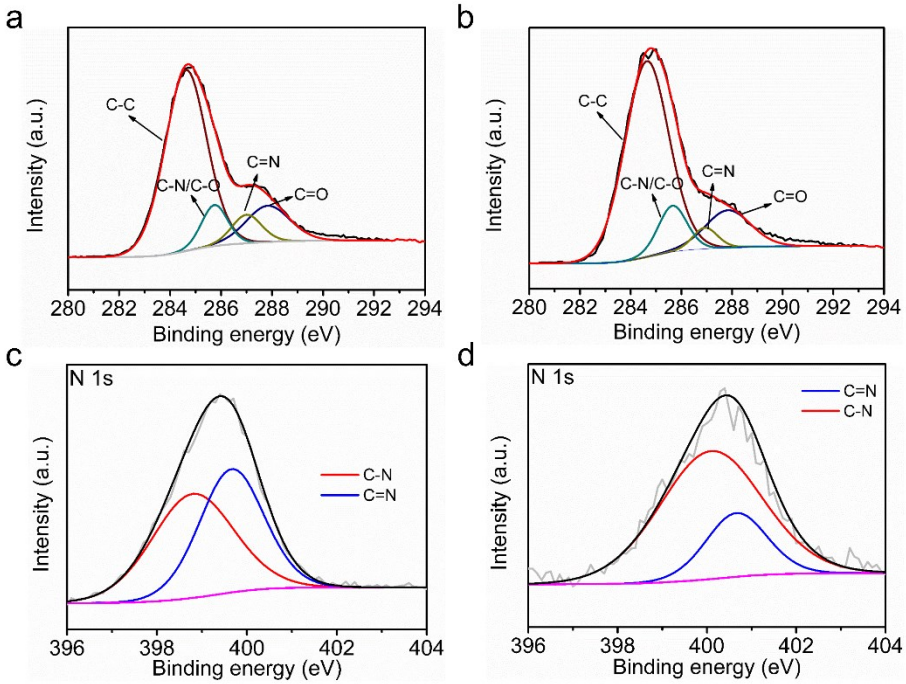

Fig. S2 (a-b) High-resolution XPS C 1s spectra of (a) the BCP and (b) the LCP; (c-d) high-resolution XPS N 1s spectra of (c) the BCP and (d) the LCP.

Table S1. Elemental analysis of two polymers.

		C	N	O	H	N/O	C=N/ C=O
BCP	Weight%	51.05	17.88	23.55	3.04	0.76	/
	Atomic ratio	4.25	1.28	1.47	3.04	0.87	0.87
LCP	Weight%	54.02	15.54	25.55	3.36	0.61	/
	Atomic ratio	4.50	1.11	1.60	3.36	0.69	0.35

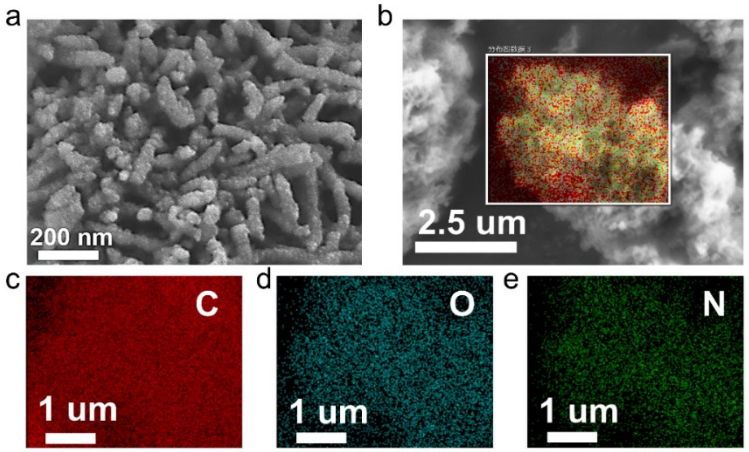

Fig. S3 (a) SEM image and (b-e) Elemental mapping (C, O, N) of the BCP.

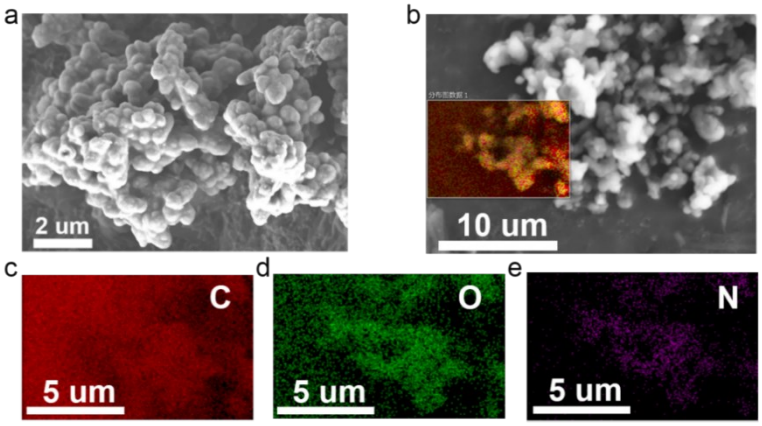

Fig. S4 (a) SEM image and (b-e) Elemental mapping (C, O, N) of the LCP.

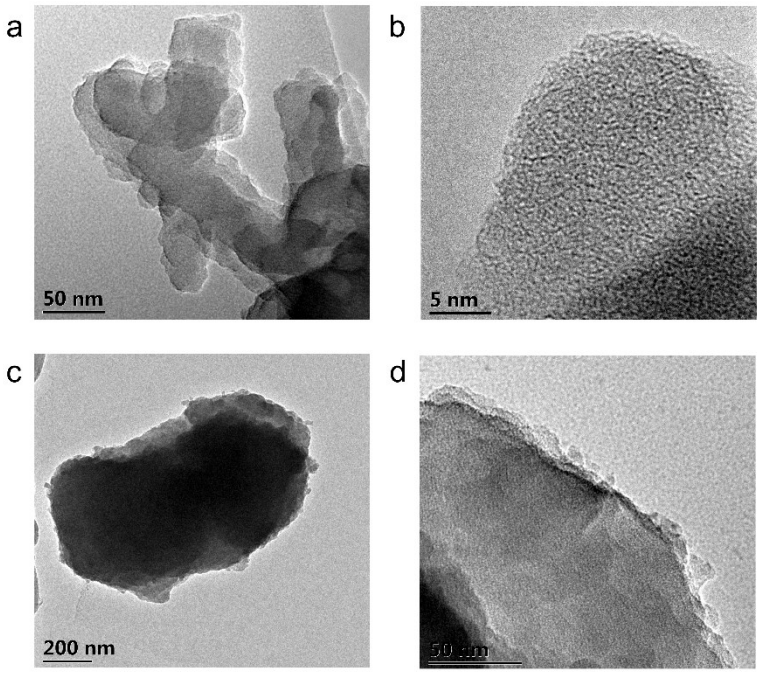

Fig. S5 TEM images of the (a-b) BCP and (c-d) LCP.

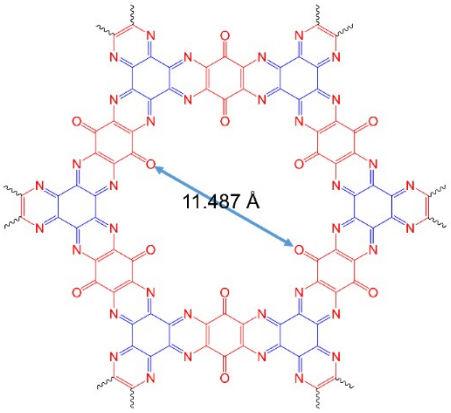

Fig. S6 The pore size of BCP with regionally regular COFs structure.

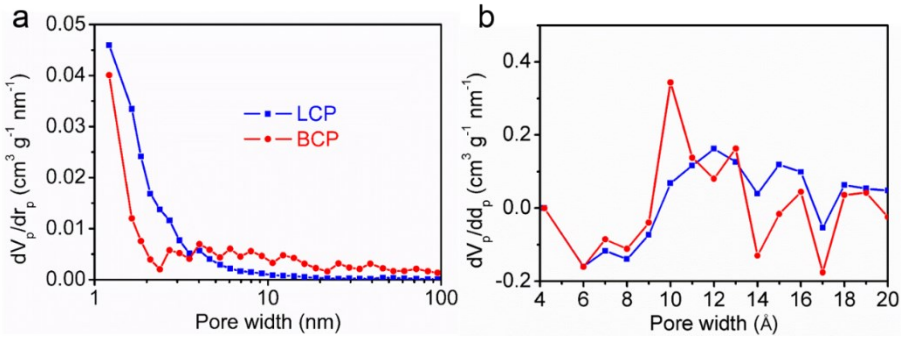

Fig. S7 Pore size distribution of two polymers. (a) BJH plot; (b) MP plot.

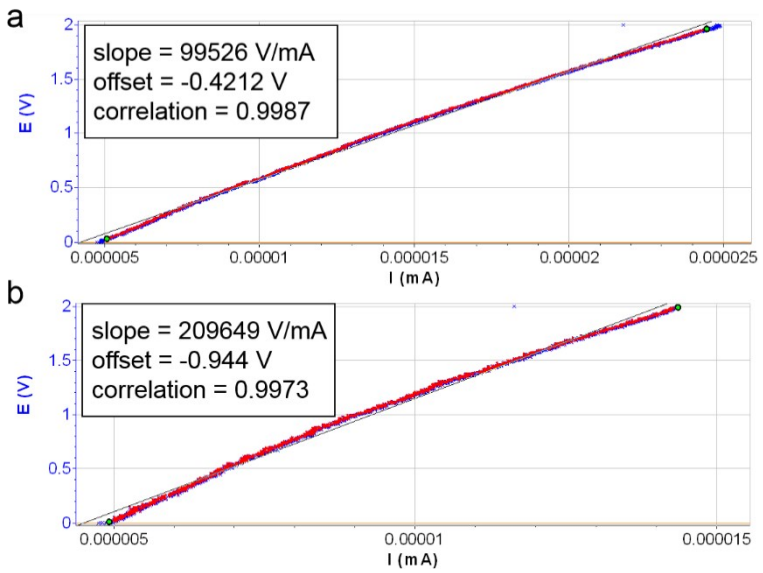

Fig. S8 I-V curves of (a) the BCP and (b) the LCP.

The electrical conductivity was measured using linear sweep voltammetry via BioLogic VMP3 potentiostat. The powder was pressed into pellet at the pressure of 20 MPa, and the pellets were sandwiched between two stainless steel gaskets for test.

Table S2. Electrical conductivity of two polymers.

Sample	R (Ω)	d (mm)	S (cm^2)	σ (S/cm)
BCP	$9.953*10^7$	0.41	1.539	$2.677*10^{-10}$
LCP	$2.097*10^8$	0.46	1.539	$1.426*10^{-10}$

The electrical conductivity can be calculated according to the following formula:

$$\sigma = \frac{d}{R \times S}$$

where R equalled the slope of the I-V curve, and S and d were the area and thickness of the pellet, respectively.

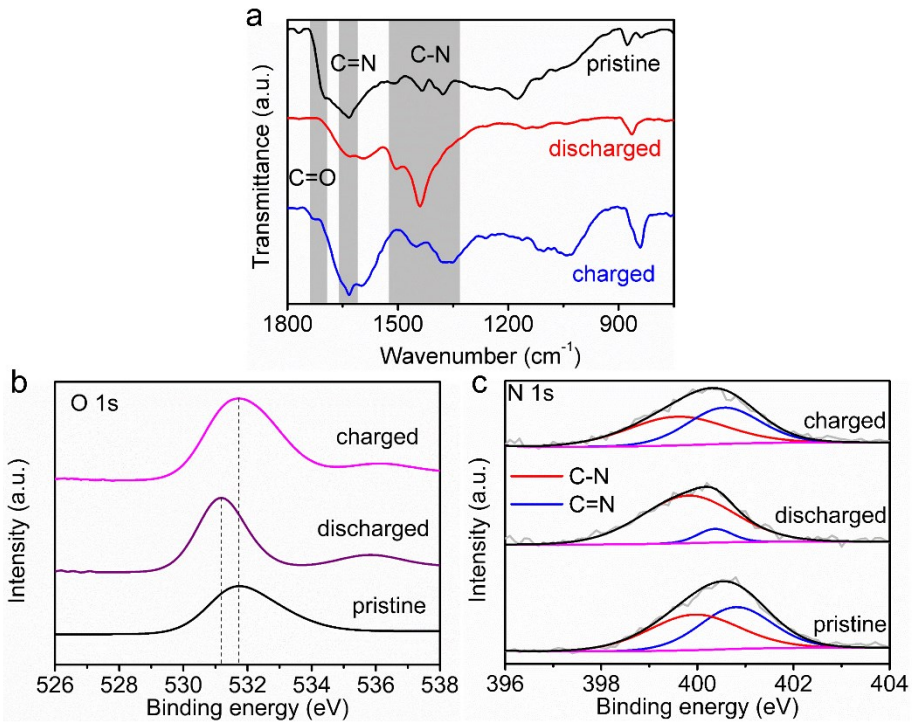

Fig. S9 (a) FITR spectra, (b) high-resolution XPS O 1s spectra, and (c) N 1s spectra of the BCP anode at different state.

To confirm the Na-storage mechanism, ex-situ FTIR and XPS tests were applied to investigate the structural changes during cycling. In view of the same Na-storage active sites in two polymers, here we only conducted tests on the BCP anode. The pristine electrode exhibited adsorption peaks at 1701 cm^{-1} in FTIR spectra (Fig. S9a), which corresponded to the stretching vibrations of C=O groups. The characteristic peak of C=O groups disappeared when being fully discharged to 0.01 V and reappeared at 1734 cm^{-1} after being recharged to 3.0 V, indicating the reversible redox process of C=O groups during cycling. In addition, the pristine electrode showed peaks in the wavenumber ranging from 1432 to 1375 cm^{-1} that can be assigned to C-N groups, which became strong at the discharged state and recovered after being recharged. Meanwhile, the featuring peak at 1630 cm^{-1} of C=N groups in the pristine electrode disappeared when being discharged to 0.01 V and then recovered at fully charged state. The evolution of C-N and C=N groups during discharge-charge process indicated the reversible Na^+ ion insertion/extraction. The same conclusions can be further verified by ex-situ high-resolution XPS spectra of O 1s and N 1s in Fig. S9b-c. In the O 1s spectra, peaks shifted to lower binding energy after discharge and returned to pristine state after charge, indicating the reversible transformation of C=O groups. Furthermore, a new peak at ~536 eV in the O 1s spectra appeared during the sodiation process, which is considered to be O-Na peak, and the intensity of the same peak became weak after the desodiation process, further illustrating the reversible Na^+ ion insertion/extraction of C=O groups. In the N 1s spectra, the intensity of C=N peak decreased and that of C-N peak increased after discharge. When being charged to 3.0 V, the peaks recovered to the pristine state on the whole.

In conclusion, according to the ex-situ FTIR and XPS spectra, the evolution of

C=O and C=N groups during discharge-charge process indicated that the C=O groups and C=N groups were redox-active centers.[1, 2]

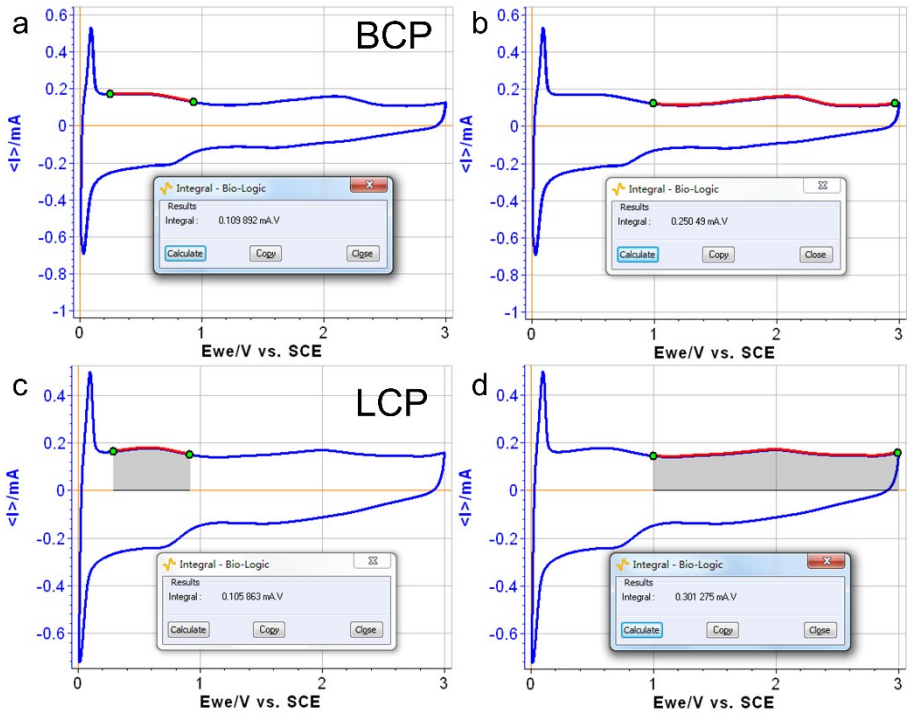

Fig. S10 The integral for the redox peaks of BCP anode (a, b) and LCP anode (c, d).

The redox peak at low potential can probably be assigned to the redox reactions of C=N groups, and the redox peaks at high potentials should be ascribed to the redox reactions of C=O groups.

For BCP anode, the ratio of the content of C=N groups to C=O groups was ~0.87 (Table S1). Besides, it has been reported that one pyrazine ring (containing two C=N groups) could insert one Na^+ ion,[3] and thus the ratio of the capacity contribution of the C=N groups and C=O groups should be ~0.44. As shown in Fig. S10a and Fig. S10b, the ratio of the integral area of the redox peaks from the C=N groups and C=O groups was also approximately 0.44.

For LCP anode, the ratio of the content of C=N groups to C=O groups was ~0.35 (Table S1). According to the structures, the ratio of the capacity contribution of the C=N groups and C=O groups should be ~0.35. As shown in Fig. S10c and Fig. S10d, the ratio of the integral area of the redox peaks from the C=N groups and C=O groups was also approximately 0.35.

All of these results indicated that the redox centers were C=N and C=O groups in both BCP and LCP.

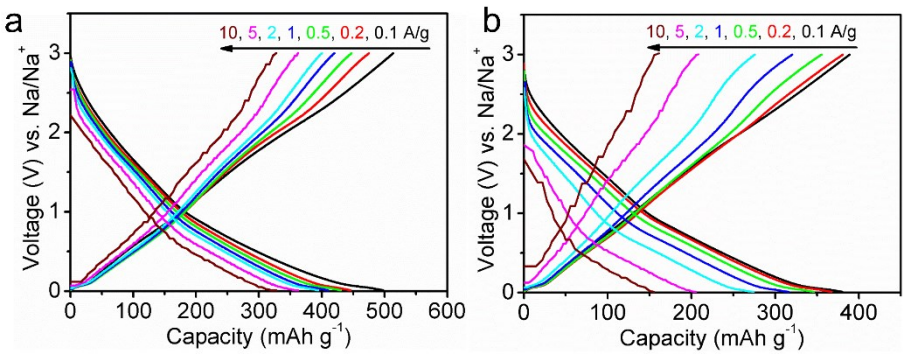

Fig. S11 Voltage-capacity profiles of the (a) BCP anode, and (b) LCP anode at different current densities.

Table S3. Comparison of the LCP and the BCP anodes with representative organic anodes for SIBs.

Active material	Content in electrode	Voltage (V)	Capacity, current density (mAh g^{-1}, A g^{-1})	Capacity retention (current density (A g^{-1}), cycle numbers)	Ref.
BCP	**50%**	**0.01-3.0**	**~450, 0.1; ~376, 5; ~330, 10**	**89.3% (0.1, 200)**	**This work**
LCP	**50%**	**0.01-3.0**	**380.3, 0.1; 205.5, 5; 155.7, 10**	**~100% (0.1, 200)**	
Na_2TP	50%	0-2.0	295, 0.03; 100, 3	90% (0.03, 90)	4
Na_2PDC	50%	0.3-2.0	270, 0.0127; 138, 1.27	83% (0.0127, 100)	5
DAAQ-COF	60%	0.05-3.0	500, 0.05; 198, 5	98% (5, 10000)	6
TFPB-TAPT COF	/	0.01-1.6	245, 0.03; 145, 0.2	51% (0.03, 500)	7
Polydopamine derivative	70%	0-3.0	433, 0.1; 122, 3.2	100% (0.05, 1000)	8
2D Polyimide nanosheet	70%	0.01-2.5	312, 0.1; 137, 10	95% (1, 1100)	9
PDCzBT	60%	0.01-3.0	145, 0.02; 99, 0.1	~100% (0.1, 200)	10
E-2D CTF	70%	0.01-2.5	262, 0.1; 119, 5	95% (1, 1200)	11
HsGDY	100%	0.005-3.0	650, 0.1; 220, 5	~100% (1, 1000)	12
cPAN-NF	60%	0.001-3.0	527, 0.05; 258, 2	99.4% (1, 3500)	1
ALP-8	60%	0.01-3.0	170, 0.0834; 57, 5.56	90% (0.0834, 150)	13
Thiocarboxylate	60%	/	567, 0.05	65% (0.5, 100)	14

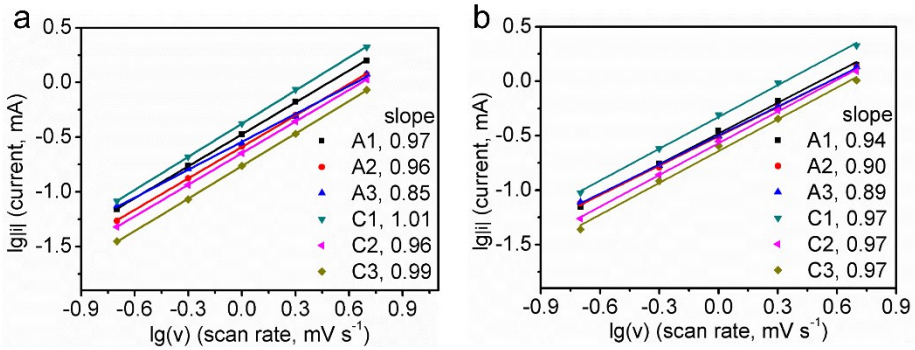

Fig. S12 log relationship between the absolute value of peak current and scan rate of the (a) BCP anode and (b) LCP anode.

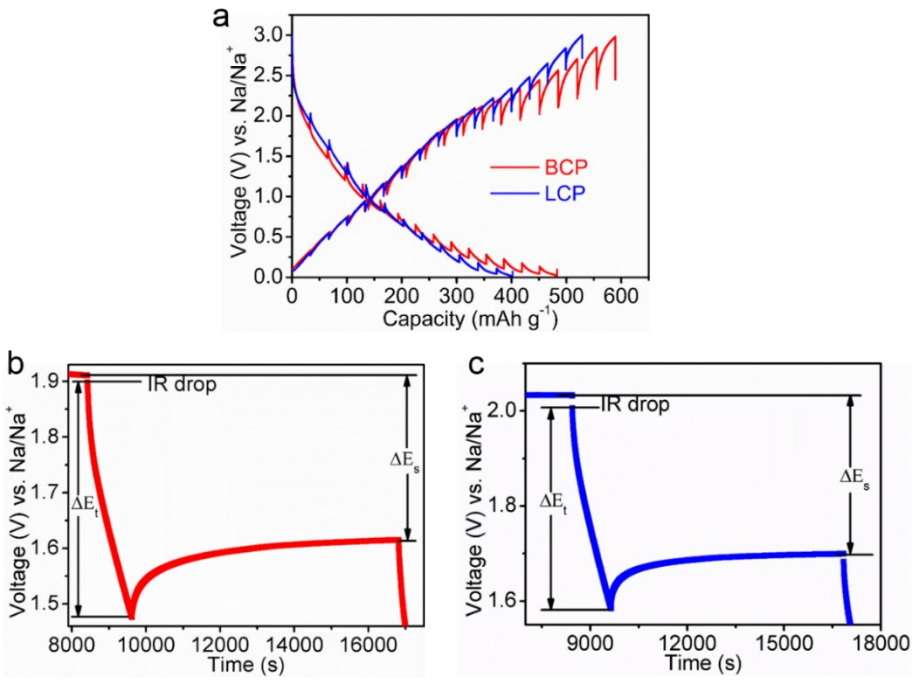

Fig. S13 (a) GITT discharge-charge profiles of two anodes; (b) a representative discharge GITT step of the BCP anode; (c) a representative discharge GITT step of the LCP anode.

The Na^+ ion diffusion coefficient (D_{Na^+}) can be calculated according to the following formula:

$$D_{Na^+} = \frac{4}{\pi\tau} \times \left(\frac{m_B V_M}{M_B S}\right)^2 \times \left(\frac{\Delta E_s}{\Delta E_t}\right)^2$$

V_M was calculated by measuring the mass and the volume of the pressed pellet, M_B was the mass of the repetitive unit, and S was the area of the pressed pellet.

Table S4. The equivalent circuit model and the fitted results.

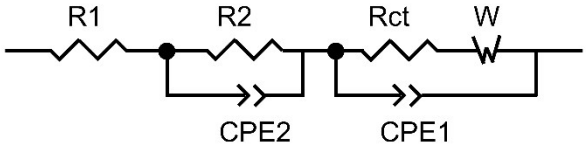

Anode	state	R_1	R_2	CPE_2	CPE_1	R_{ct}	W
BCP	1st discharge	2.187	1.293	0.611	0.922	1.443	0.396
	50th discharge	4.358	0.210	1.457	0.517	19.02	0.372
LCP	1st discharge	1.688	31.45	0.338	0.791	4.577	0.457
	50th discharge	1.568	12.31	0.514	0.810	30.93	0.421

References

1. T. Gu, M. Zhou, B. Huang, M. Liu, X. Xiong, K. Wang, S. Cheng and K. Jiang, *J. Mater. Chem. A*, 2018, **6**, 18592-18598.
2. Y. Chen, H. Li, M. Tang, S. Zhuo, Y. Wu, E. Wang, S. Wang, C. Wang and W. Hu, *J. Mater. Chem. A*, 2019, **7**, 20891-20898.
3. R. Shi, L. Liu, Y. Lu, C. Wang, Y. Li, L. Li, Z. Yan and J. Chen, *Nat. Commun.*, 2020, **11**, 178.
4. Y. Park, D.-S. Shin, S. H. Woo, N. S. Choi, K. H. Shin, S. M. Oh, K. T. Lee and S. Y. Hong, *Adv. Mater.*, 2012, **24**, 3562-3567.
5. H. Padhy, Y. Chen, J. Lüder, S. R. Gajella, S. Manzhos and P. Balaya, *Adv. Energy Mater.*, 2018, **8**, 1701572.
6. S. Gu, S. Wu, L. Cao, M. Li, N. Qin, J. Zhu, Z. Wang, Y. Li, Z. Li, J. Chen and Z. Lu, *J. Am. Chem. Soc.*, 2019, **141**, 9623-9628.
7. B. C. Patra, S. K. Das, A. Ghosh, A. Raj K, P. Moitra, M. Addicoat, S. Mitra, A. Bhaumik, S. Bhattacharya and A. Pradhan, *J. Mater. Chem. A*, 2018, **6**, 16655-16663.
8. T. Sun, Z.-j. Li, H.-g. Wang, D. Bao, F.-l. Meng and X.-b. Zhang, *Angew. Chem. Int. Ed.*, 2016, **128**, 10820-10824.
9. H. Duan, P. Lyu, J. Liu, Y. Zhao and Y. Xu, *ACS Nano*, 2019, **13**, 2473-2480.
10. S. Zhang, W. Huang, P. Hu, C. Huang, C. Shang, C. Zhang, R. Yang and G. Cui, *J. Mater. Chem. A*, 2015, **3**, 1896-1901.
11. J. Liu, P. Lyu, Y. Zhang, P. Nachtigall and Y. Xu, *Adv. Mater.*, 2018, **30**, 1705401.
12. J. He, N. Wang, Z. Cui, H. Du, L. Fu, C. Huang, Z. Yang, X. Shen, Y. Yi, Z. Tu and Y. Li, *Nat. Commun.*, 2017, **8**, 1172.
13. K. S. Weeraratne, A. A. Alzharani and H. M. El-Kaderi, *ACS Appl. Mater. Interfaces*, 2019, **11**, 23520-23526.
14. H. Zhao, J. Wang, Y. Zheng, J. Li, X. Han, G. He and Y. Du, *Angew. Chem. Int. Ed.*, 2017, **56**, 15334-15338.